physics

MDPI

Article

Critical Angle Refractometry for Lossy Media with a Priori Known Extinction Coefficient

Spyridon Koutsoumpos, Panagiotis Giannios † and Konstantinos Moutzouris *

Laboratory of Electronic Devices and Materials, Department of Electrical & Electronic Engineering, University of West Attica, 12244 Egaleo, Greece; skoutsoumpos@uniwa.gr (S.K.); panagiotis.giannios@irbbarcelona.org (P.G.)
* Correspondence: moutzouris@uniwa.gr
† Current address: Barcelona Institute of Science and Technology, Institute for Research in Biomedicine (IRB), 08028 Barcelona, Spain.

Abstract: Critical angle refractometry is an established technique for determining the refractive index of liquids and solids. For transparent samples, the critical angle refractometry precision is limited by incidence angle resolution. For lossy samples, the precision is also affected by reflectance measurement error. In the present study, it is demonstarted that reflectance error can be practically eliminated, provided that the sample's extinction coefficient is a priori known with sufficient accuracy (typically, better than 5%) through an independent measurement. Then, critical angle refractometry can be as precise with lossy media as with transparent ones.

Keywords: optical instruments; refractive index; critical angle refractometry

check for updates

Citation: Koutsoumpos, S.; Giannios, P.; Moutzouris, K. Critical Angle Refractometry for Lossy Media with a Priori Known Extinction Coefficient. *Physics* **2021**, *3*, 569–578. https://doi.org/10.3390/physics3030036

Received: 4 June 2021
Accepted: 22 July 2021
Published: 3 August 2021

1. Introduction

Critical angle refractometry is the standard for determining the refractive index of transparent media [1–6]. The method relies on measurements of the reflectance, $R(\theta)$, of the interface, formed by a transparent front medium (which is commonly a prism) of known refractive index, n_o, and the sample of unknown index, n, for a range of incidence angles, θ, that includes the critical angle, θ_c, of total internal reflection (TIR) [7–9].

As it is shown in Figure 1, the critical angle is located at a sharp discontinuity of the θ-derivative, $R'(\theta)$; the refractive index of the sample is obtained from the TIR condition:

$$n/n_o = \sin\theta_c, \tag{1}$$

with the corresponding relative error:

$$\delta n/n = \delta\theta_c/\tan\theta_c. \tag{2}$$

In determining the TIR critical angle, the error, $\delta\theta_c$, is mainly regulated by the angular resolution of the experimental setup, which is typically between 20 µrad and 100 µrad for state-of-the-art refractometers [10].

Critical angle refractometry has also been used with lossy media where the refractive index turns into the complex number, $n = n_r + in_i$, the imaginary part of which (imaginary index) incorporates loss effects, namely, absorption and/or scattering. The reflectance profile, $R(\theta)$, becomes smoother, and the critical angle, θ_c, is located at the maximum of $R'(\theta)$, which now marks the gradual transition from the attenuated TIR (a-TIR) to the partial reflection regime; see Figure 1. The underlying assumption is that Equation (1) is still valid (at least approximately) and that it can be used to obtain an estimate of the real index of the lossy sample [11,12]. This assumption introduces systematic errors that have been the subject of extensive discussion; see, e.g., [13–15] Let us note that fitting the reflectance profile, $R(\theta)$, to Fresnel equations is another way to compute the complex optical constants [16–18]. However, bearing its own strengths and weaknesses, data regression is

not a point method and, thus, cannot be taken as a "critical angle" refractometry approach in itself.

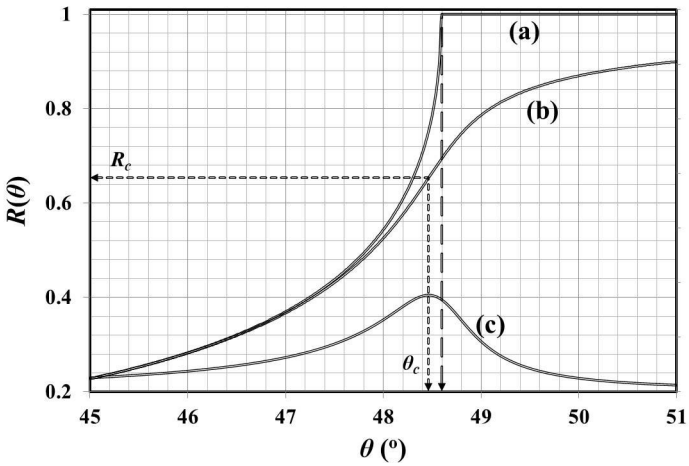

Figure 1. (**a**) Fresnel reflectance, $R(\theta)$, profile, as a function of the incidence angle, θ, at an interface between a transparent sample and a transparent prism, such that the ratio of unknown refractive index to the known index is $n/n_o = 0.75$. Long-dashed arrow indicates the location of the corresponding critical angle, θ_c. (**b**) Fresnel reflectance profile at an interface between a lossy sample and a transparent prism, such that $n_r/n_o = 0.75$ and $n_i/n_o = 0.005$, where n_r and n_i are the real and inginary parts of the refractive index, respectively. Short-dashed arrows indicate the location of the corresponding critical angle and critical reflectance, R_c. (**c**) The critical angle rests at the peak of the reflectance derivative, which is also depicted (in arbitrary units).

Recently, the universal condition of a-TIR,

$$n_r/n_o = g_1(\theta_c, R_c) \quad \text{and} \quad n_i/n_o = g_2(\theta_c, R_c), \tag{3}$$

was proposed, where R_c is the critical reflectance at θ_c, and functions g_1 and g_2 are derived from the Fresnel equations [19]. In the case of the s-polarisation, which is the main foucus of the present study, these equations are given in Section 2. Using Equation (3), the complex refractive index can be determined by θ_c and R_c.

Then, the relative error of the real index, $\delta n_r/n_r$, depends on both $\delta\theta_c$ and δR_c:

$$\frac{\delta n_r}{n_r} = \frac{1}{g_1} \cdot \sqrt{\left(\frac{\partial g_1}{\partial \theta_c} \cdot \delta\theta_c\right)^2 + \left(\frac{\partial g_1}{\partial R_c} \cdot \delta R_c\right)^2}. \tag{4}$$

In determining the critical reflectance, the error δR_c is mainly due to intensity fluctuations of the laser sources and, therefore, to be of the order of 10^{-2}, which is at least two orders of magnitude larger than $\delta\theta_c$. As a result, critical angle refractometry is less precise with lossy media than it is with transparent ones.

In this paper, it is demonstrated that the critical reflectance can be numerically computed with higher accuracy than it can be experimentally obtained, provided that the extinction coefficient of the sample is a priori known with sufficient accuracy (<5%, typically). Then, the real index relative error for lossy samples (being $\delta\theta_c$ and δR_c dependent; see Equation (4)) can become equal to the relative error for transparent samples (which is only $\delta\theta_c$ dependent; see Equation (2)). This is a significant advancement in the field of optical characterisation of absorbing and/or scattering media, which include, among others, various forms of biological matter, non-transparent liquids, colloids and food products.

2. Background Theory and Initial Observations

The functions g_1 and g_2 [19] are compactly expressed in terms of the sample's complex dielectric constant, $\epsilon_r + i \cdot \epsilon_i = (n_r + i \cdot n_i)^2$, and the prism's dielectric constant, $\epsilon_o = n_p^2$:

$$g_1 = \left[\frac{\sqrt{\epsilon_r^2 + \epsilon_i^2}}{2\epsilon_o} + \frac{\epsilon_r}{2\epsilon_o} \right]^{1/2} \quad \text{and} \quad g_2 = \left[\frac{\sqrt{\epsilon_r^2 + \epsilon_i^2}}{2\epsilon_o} - \frac{\epsilon_r}{2\epsilon_o} \right]^{1/2}, \tag{5}$$

where

$$\frac{\epsilon_r}{\epsilon_o} = \frac{\alpha + t^2}{1 + t^2} \quad \text{and} \quad \frac{\epsilon_i}{\epsilon_o} = \frac{\sqrt{\gamma^2 - \alpha^2}}{1 + t^2}, \tag{6}$$

with

$$\alpha = \frac{(1+\gamma)^2}{2\rho^2} - \gamma, \qquad \gamma = \frac{2t}{(3\rho^2 - 2\rho - 2)t + \rho\sqrt{(9\rho^2 - 12\rho - 8)t^2 - 4}}, \tag{7}$$

and

$$t = \tan\theta_c, \qquad \rho = \frac{1 + R_c}{1 - R_c}. \tag{8}$$

As it is described in [19], the preceding formalism, which is valid for s-polarisation, calculates output values (n_r, n_i) from refractometric input pairs (θ_c, R_c) by successive algebraic substitutions into Equations (5)–(8). Let us remark that Equations (5) and (6) are also valid for p-polarised light, in which case however, there exist no explicit solutions for α and γ such as those provided by Equation (7). Instead, these parameters can be calculated as solutions to two algebraic equations, as is analytically shown in [19]. In that sense, the forthcoming analysis may be replicated for p-polarisation. Despite some more complication in the calculations, the results, reported here for s-polarisation, are qualitatively similar to those of p-polarisation.

Figure 2 gives a graphical insight by the isoangular curve which consists of pairs $(n_r/n_o,\ n_i/n_o)$, computed by keeping θ_c constant ($\theta_c = \pi/4$ in this example), while letting R_c to vary. There is no loss of generality, associated with the specific choice of θ_c, because larger (smaller) critical angles simply shift the curve to the right (left). An indicative measurement (with $\theta_c = \pi/4, R_c$ varying) defines a single point in the $(n_r/n_o,\ n_i/n_o)$-plane, whose coordinates uniquely determine the complex refractive index.

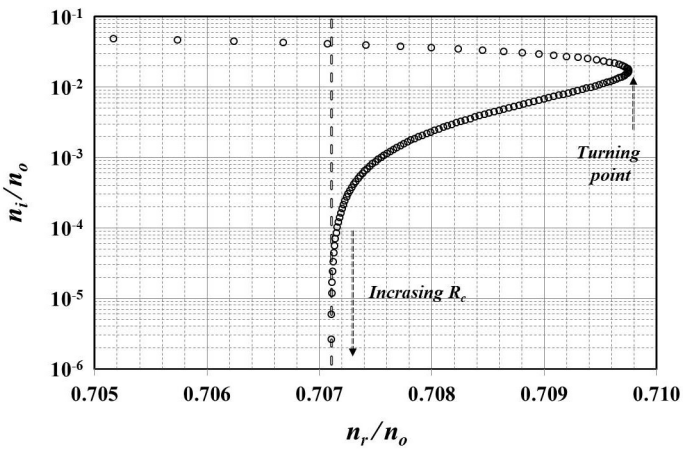

Figure 2. Isoangular curves in the $(n_r/n_o,\ n_i/n_o)$-plane for the s-polarisation, $\theta_c = \pi/4$ and variable R_c. As one moves along the direction of the arrow, R_c increases in steps of 0.005, within the range $[0.385, 0.990]$. The vertical dashed line marks the transparency limit, $n_r/n_o = \sin(\pi/4)$.

In Figure 2, one can observe quite wide range, spanned by the imaginary index as the critical reflectance varies, especially compared to the relatively modest shift for the

real index, which is nevertheless non-negligible. The vertical dashed line in Figure 2 marks the transparency limit $n_r/n_o = \sin(\pi/4) \approx 0.707$, which is the estimate of the TIR-condition (Equation (1)) for each point of the isoangular curve. Unsurprisingly, this estimate practically coincides with the exact result for small n_i/n_o, e.g., $n_i/n_o \ll 10^{-4}$, a range that includes, for example, most liquids at wavelengths far from their ultraviolet or infrared resonances, but excludes most forms of biological matter, even in the therapeutic optical window. The most interesting feature in Figure 2 is the turning point of the isoangular curve, which vividly demonstrates that the systematic error, introduced by use of Equation (1) with lossy media, does not increase monotonically with attenuation but decreases above the turning point, and even becomes zero when the isoangular curve crosses the transparency limit marked by the dashed vertical line. This behaviour, which now emerges as a natural consequence of the universal a-TIR condition, had been previously observed [13,20] and labeled as inexplicable by other authors [14].

3. Method's Application with a Priori Known Extinction Coefficient

3.1. Main Concept

The sample's extinction coefficient, μ, i.e., the sum of the absorption coefficient, μ_a, and the scattering coefficient, μ_s, can be a priori known via an independent experimental method such as absorption spectroscopy or collimated transmittance spectroscopy. This type of independent extinction coefficient measurement has been reported earlier for pure water [21], various emulsions [22], bioliquids [23], oils [24] and semiconductors [25]; typically, the relative error, $\sigma_\mu = \delta\mu/\mu$, in the measurement of the extinction coefficient is of 0.1% to 10% [26–30].

The formalism, described in Section 2, can be used to calculate the real part of the refractive index (real index) from the value of the critical angle alone. The direct measurement of critical reflectance is no longer needed, since R_c can be determined from the value of the extinction coefficient, which is related to the imaginary index [31]:

$$\mu = \frac{4\pi n_i}{\lambda}, \tag{9}$$

so that the following equation holds true (λ is the light wavelength):

$$g_2(\theta_c, R_c) = \frac{n_i}{n_o} = \frac{\mu\lambda}{4\pi n_o}. \tag{10}$$

Solving Equation (10) for R_c (the only unknown variable) is a simple task for iterative computing software such as *Mathematica*'s `FindRoot` or *Mathcad*'s `Find`. As long as the initial guess root is kept within its physically meaningful range, $0 < R_c < 1$, the solution is always unique and unambiguous. Substituting the measured value of θ_c and the numerically retrieved value of R_c in $g_1(\theta_c, R_c)$ yields the real index of the lossy sample.

The procedure described has a straightforward graphical interpretation. Let us consider the measurement of a critical angle, for example, $\theta_c = \pi/4$, so that one can refer to Figure 2. An a priori known value of the extinction coefficient (equivalently, n_i) defines a unique horizontal line that crosses the isoangular curve at a single point; locating its position is equivalent to numerically computing the value of R_c. The abscissa of that point is the real index of the lossy medium.

3.2. Critical Reflectance Error

The formalism of Section 2 enables the calculation of n_r from the values of θ_c and R_c. The method, introduced in Section 3.1, retrieves the numerical value of R_c from the extinction coefficient (when the extinction coefficient is already known) instead of its direct measurement. To better appreciate the advantage of the proposed method, one has to remember that the experimental error of a direct reflectance measurement is typically greater than 10^{-2}. Breaking this threshold does not seem possible with standard unstabilized laser sources of moderate cost, such as those used in common refractometers.

Let us now show that the propagated error, δR_c, of the numerically retrieved R_c can be kept below the 10^{-2} threshold. To this end, one accounts for the fact that R_c is numerically computed from input values of θ_c and μ, or equivalently, θ_c and n_i, which are assumed to be independent variables, so that the covariance between them can be taken to be zero. Therefore, propagated error δR_c conveys corresponding experimental errors $\delta\theta_c$ and δn_i:

$$\delta R_c = \sqrt{\left(\frac{\partial R_c}{\partial \theta_c} \cdot \delta\theta_c\right)^2 + \left(\frac{\partial R_c}{\partial n_i} \cdot \delta n_i\right)^2}. \tag{11}$$

Critical reflectance, R_c, is not expressed explicitly as a function of θ_c and n_i. Instead, Equation (10) can be restated in the implicit form: $F(\theta_c, R_c, n_i) = F(g_2(\theta_c, R_c), n_i) = g_2(\theta_c, R_c) - n_i/n_o = 0$. Then, the derivatives in Equation (11) can be obtained using the implicit function theorem:

$$\frac{\partial R_c}{\partial \theta_c} = -\left(\frac{\partial F}{\partial \theta_c}\right) \Big/ \left(\frac{\partial F}{\partial R_c}\right) = -\left(\frac{\partial g_2}{\partial \theta_c}\right) \Big/ \left(\frac{\partial g_2}{\partial R_c}\right), \tag{12}$$

and

$$\frac{\partial R_c}{\partial n_i} = -\left(\frac{\partial F}{\partial n_i}\right) \Big/ \left(\frac{\partial F}{\partial R_c}\right) = \frac{1}{n_o} \Big/ \left(\frac{\partial g_2}{\partial R_c}\right). \tag{13}$$

Moreover, one can introduce the relative error, σ_μ, which is related to δn_i and $\delta\mu$:

$$\sigma_\mu = \frac{\delta\mu}{\mu} = \frac{\delta n_i}{n_i} = \frac{\delta n_i}{g_2 \cdot n_o}. \tag{14}$$

Substituting Equations (12)–(14) into Equation (11) yields:

$$\delta R_c = \left|\frac{\partial g_2}{\partial R_c}\right|^{-1} \sqrt{\left(\frac{\partial g_2}{\partial \theta_c} \cdot \delta\theta_c\right)^2 + (\sigma_\mu \cdot g_2)^2}. \tag{15}$$

Values of g_2 and its two partial derivatives that appear in Equation (15) can be easily computed for any pair (θ_c, R_c). Therefore, error δR_c can be estimated as a function of the variables $\theta_c, R_c, \delta\theta_c$, and σ_μ. Numerical investigation reveals that δR_c is practically independent of $\delta\theta_c$, at least when this parameter is kept within its reasonable range, 20 μrad $\leq \delta\theta_c \leq$ 100 μrad. This observation reflects the easily verifiable fact that

$$\frac{\partial g_2}{\partial \theta_c} \cdot \delta\theta_c \ll \sigma_\mu \cdot g_2, \tag{16}$$

which reduces Equation (15) to the approximate form:

$$\delta R_c \approx \left|\frac{\partial g_2}{\partial R_c}\right|^{-1} \cdot \sigma_\mu \cdot g_2, \tag{17}$$

and narrows δR_c down to a function of only three variables, namely, of θ_c, R_c, and σ_μ.

Figure 3 shows the results of calculations of δR_c versus σ_μ for indicative values $\theta_c = \pi/4$ and $R_c = 0.5$: the solid line, produced via the exact Equation (15). In agreement with the approximate Equation (17), δR_c is not affected by $\delta\theta_c$ and increases linearly with σ_μ, which is taken within the range $0.1\% \leq \sigma_\mu \leq 10\%$. One can observe that $\delta R_c \approx 10^{-4}$ (or 10^{-3}) when $\sigma_\mu \approx 0.1\%$ (1%), indicating that critical reflectance error can be two (one) orders of magnitude smaller than the 10^{-2} threshold, when R_c is numerically retrieved from the a priori known extinction coefficient.

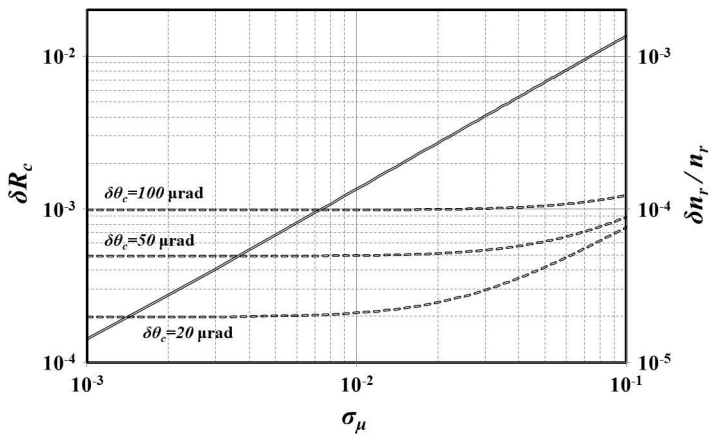

Figure 3. Solid line: error in the numerical determination of the critical reflectance, δR_c, as a function of the exstinction coefficient relative error, σ_μ. Calculations are based on Equation (15) for $\theta_c = \pi/4$ and $R_c = 0.5$. Dashed lines: relative error, $\delta n_r/n_r$, as a function of σ_μ for the same pair of θ_c and R_c values; $\delta\theta_c$ varies from 100 via 50 to 20 µrad, as indicated. Calculations result from substituting Equation (15) into Equation (4).

3.3. Real Index Error

The relative error, $\delta n_r/n_r$, can be computed as a function of the variables $\theta_c, R_c, \delta\theta_c$, and σ_μ by substituting Equation (15) into Equation (4).

Figure 3 shows $\delta n_r/n_r$ versus σ_μ for $\theta_c = \pi/4$ and $R_c = 0.5$: the dashed lines correspond to $\delta\theta_c = 100, 50$ and 20 µrad, as indicated. The error lines become horizontal for small σ_μ at a constant value $\delta n_r/n_r \approx \delta\theta_c/\tan\theta_c$ (in this example, $\tan\theta_c = 1$). In the horizontal region, the relative real index error is practically equal to that of a transparent sample (cf. Equation (2)). This observation alone proves that refractometry with lossy media can be as precise as the refractometry with transparent ones, provided that the extinction coefficient is a priori known with sufficient accuracy. The horizontal regions terminate at a maximum permissible σ_μ, above which $\delta n_r/n_r$ continues to increase beyond the transparency limit. In the example considered, this transition occurs in the vicinity of $\sigma_\mu \approx 1\%$ when $\delta\theta_c = 20$ µrad, at $\sigma_\mu \approx 2\%$ when $\delta\theta_c = 50$ µrad, and at $\sigma_\mu \approx 4\%$ when $\delta\theta_c = 100$ µrad.

Note that the upper and lower dashed lines in Figure 3 flatten out at $\delta n_r/n_r \approx 10^{-4}$ (when $\delta\theta_c = 100$ µrad) and $\delta n_r/n_r \approx 2 \times 10^{-5}$ (when $\delta\theta_c = 20$ µrad). These levels match the specifications of modern refractometers operating with transparent samples, which typically prescribe an error $\delta n/n$ between $\sim 10^{-4}$ (standard precision) and $\sim 2 \times 10^{-5}$ (ultimate precision) [32].

As a final exercise, let us consider the refractometric measurement of a lossy sample with $n_r = 1.5$ by use of a reference front medium with $n_o = 2$, so that $n_r/n_o = 0.75$. With these assumptions, as given, it is straightforward to calculate the magnitude of σ_μ that is required to reach (i) the ultimate precision $\delta n_r/n_r \approx 2 \times 10^{-5}$, assuming that the refractometer measures critical angles with an ultrahigh accuracy $\delta\theta_c = 20$ µrad, and (ii) a standard precision $\delta n_r/n_r \approx 10^{-4}$, with a more tolerant $\delta\theta_c = 100$ µrad. The calculations are shown in Figure 4 by solid and dashed lines, respectively.

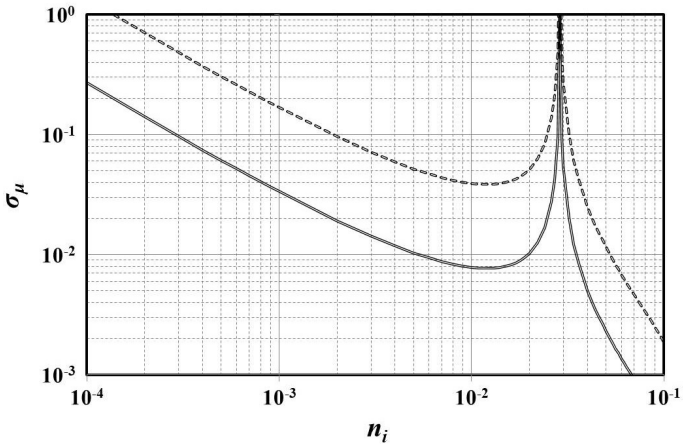

Figure 4. Maximum permissible relative error, σ_μ, as a function of n_i for ultimate refractometric precision $\delta n_r/n_r = 2 \times 10^{-5}$, when $\delta\theta_c = 20$ µrad (solid line), and standard refractometric precision $\delta n_r/n_r = 10^{-4}$, when $\delta\theta_c = 100$ µrad (dashed line). A sample with $n_r = 1.5$ and a prism with $n_o = 2$ are considered.

Therein, one observes a general trend: the maximum permissible σ_μ decreases with increasing n_i. This trend clearly indicates that the need for accurate measurements of the extinction coefficient is more acute when optical loss is growing. There is one exception to this, which manifests itself as a characteristic sharp peak at larger n_i. This peak reflects the vertical slope of the isoangular curve at the turning point, see Figure 2. Quite naturally, σ_μ is found increasing again at the transparent limit, where the slope of the isoangular curve is again nearly vertical. Likewise, σ_μ decreases rapidly for larger n_i after the peak because the slope of isoangular curve above there is zero

To better understand the interpretation made, let us point that a vertical slope in Figure 2 suggests that small enough change in the imaginary index causes zero shift to the real index. Similarly, a horizontal slope suggests that small change in the imaginary index causes a maximum shift in the real index. Hence, the real index error minimizes (and the maximum permissible σ_μ maximizes) as soon as the slope turns vertical, and vice versa.

Meantime, the most important observation in Figure 4 is that the real index of the sample can be measured with an extreme precision, $\delta n_r/n_r \approx 2 \times 10^{-5}$, as long as $n_i < 10^{-1}$ and $\sigma_\mu \approx 0.1\%$ (solid line). Note that although being strict, this situation is indeed realistic. For example, the extinction coefficient of water has been measured with a relative error even less than 0.1% near its infrared absorption peak (at $\lambda = 1410$ nm), where $n_i = 2.3675 \times 10^{-4}$ [21]; see discussion in Section 3.4 below. This is also possible with a much more lax $\sigma_\mu \approx 1\%$ for all $n_i < 10^{-2}$. An adequate for many applications error $\delta n_r/n_r \approx 10^{-4}$ is reached with $\sigma_\mu \approx 4\%$ for all $n_i < 4 \times 10^{-2}$ (dashed line). These observations illustrate the functionality of the proposed method with all but the most extremely attenuating media.

3.4. Comments on Implementation Issues

The proposed method involves the tandem use of two instruments. The first determines the reflectance profile at the sample's interface with a prism; prism coupling refractometers operate routinely in various laboratories and they are also commercially available; see, e.g. *Metricons*'s `2010/M` model. The second measures the sample's extinction coefficient. Collimated transmittance setups (typically, homemade) suit ideally this purpose; see, e.g., [21,26,27]. The corresponding operating principle is straightforward. The transmitted portion of a collimated light beam, travelling through sample sections of variable length, is monitored; the extinction coefficient is then deduced by fitting experimental results to the known Lambert-Beer law. This technique is commonly used for fluids where liquid cells of different sizes facilitate tuning of the path length. The technique is also applicable for solid samples, provided that slices of variable thickness can be cut.

This tandem measurement is actually known. In [21], the (real) refractive index and the extinction coefficient of several types of liquids, including water, were measured by the combined use of critical angle refractometetry and collimated transmittance spectroscopy. Unaware of the attenuated-TIR condition (Equation (3)) at that time, the standard TIR law of transparent media (Equation (1)) was exploited in [21] to determine the real index. Let us see, through a didactic example, how the method, proposed in this paper, adjusts those results.

Let us start by selecting the reported data for water at a wavelength $\lambda = 1410$ nm, where the extinction coefficient, $\mu = 21.1$ cm^{-1}, was measured [21] translating via Equation (9) into the imaginary index, $n_i = 2.3675 \times 10^{-4}$. The relative error in this measurement was as small as $\sigma_\mu = 0.05\%$. Using an SF13 glass prism with $n_o = 1.7068$, the real index was approximated by the standard TIR condition, leading to the value $n_r = 1.3183$, which, given the index of the prism, corresponds to the critical angle $\theta_c = 50.568°$.

Using the required input pair ($\theta_c = 50.568°, \mu = 21.1$ cm^{-1}), the method, proposed in the current paper, yields, first, the critical reflectance $R_c = 91.99\%$ and, then, the real index of water, corrected to a new value, $n_r = 1.31842$. The correction from the previous estimate ($n_r = 1.3183$) is relatively modest, while non negligible for applications requiring high accuracy. The modest correction effect is expected (cf. Figure 2), since the imaginary index in our example just exceeds 10^{-4}; it would have been much stronger, had the sample been more attenuating.

Using Equation (15), the prescribed $\sigma_\mu = 0.05\%$ value, combined with an assumed error in the measurement of critical angle, 20 µrad $\leq \delta\theta_c \leq$ 100 µrad, leads to a propagated error in the numerical estimation of the critical reflectance within $\delta R_c \approx 0.002\%$. Such an accuracy is surely orders of magnitude higher than the ∼1% uncertainty with which critical reflectance can be directly measured. This finding manifests the main advantage of the method here described. Then, within the same $\delta\theta_c$ range, this method yields the real index with an error of $2 \times 10^{-5} \leq \delta n_r \leq 1 \times 10^{-4}$, the latter calculated as it is described in Section 3.3. It is worth noticing the compliance of this result with Figure 3.

4. Conclusions

In this paper, the universal attenuated total internal reflection (a-TIR) condition is exploited in order to accurately determine the real part of the refractive index), n_r, of lossy media from the critical incidence angle, θ_c, at *s*-polarisation given the extinction coefficient, μ. This is accomplished in a two-step procedure. First, the critical reflectance, R_c, is numerically retrieved from the pair (θ_c, μ). Then, the real index is calculated from θ_c and R_c.

Numerical investigation reveals that R_c can be recovered (in the first step) more accurately than it can be directly measured. As a consequence the determination of the real index (in the second step) becomes more precise. The relative error, $\delta n_r / n_r$, can be reduced down to 2×10^{-5} when the respective error in the independent measurement of μ is in the range of 0.1% to 1%.

The results, obtained here, demonstrate that refractometry of lossy media can be as precise as with transparent media, a development that is of interest to various applications in biomedical optics, material characterisation, analytical chemistry and quality control.

Author Contributions: Conceptualization, K.M.; methodology, S.K., K.M.; validation, P.G., S.K.; investigation, S.K., K.M.; writing—original draft preparation, S.K., P.G.; writing—review and editing, K.M. All authors have read and agreed to the published version of the manuscript.

Funding: This research received no external funding.

Data Availability Statement: Data supporting this article are available from the corresponding author upon reasonable request.

Conflicts of Interest: The authors declare no conflict of interest.

References

1. Castrejón-Pita, J.R.; Morales, A.; Castrejón-García, R. Critical angle laser refractometer. *Rev. Sci. Instrum.* **2006**, *77*, 035101. [CrossRef]
2. Moutzouris, K.; Hloupis, G.; Stavrakas, I.; Triantis, D.; Chou, M.H. Temperature-dependent visible to near-infrared optical properties of 8 mol% Mg-doped lithium tantalate. *Opt. Mater. Express* **2011**, *1*, 458. [CrossRef]
3. Moutzouris, K.; Stavrakas, I.; Triantis, D.; Enculescu, M. Temperature-dependent refractive index of potassium acid phthalate (KAP) in the visible and near-infrared. *Opt. Mater.* **2011**, *33*, 812–816. [CrossRef]
4. Moutzouris, K.; Papamichael, M.; Betsis, S.C.; Stavrakas, I.; Hloupis, G.; Triantis, D. Refractive, dispersive and thermo-optic properties of twelve organic solvents in the visible and near-infrared. *Appl. Phys. B* **2013**, *116*, 617–622. [CrossRef]
5. Dongare, M.; Buchade, P.; Shaligram, A. Refractive index based optical Brix measurement technique with equilateral angle prism for sugar and Allied Industries. *Optik* **2015**, *126*, 2383–2385. [CrossRef]
6. Chiappe, C.; Margari, P.; Mezzetta, A.; Pomelli, C.S.; Koutsoumpos, S.; Papamichael, M.; Giannios, P.; Moutzouris, K. Temperature effects on the viscosity and the wavelength-dependent refractive index of imidazolium-based ionic liquids with a phosphorus-containing anion. *Phys. Chem. Chem. Phys.* **2017**, *19*, 8201–8209. [CrossRef] [PubMed]
7. Chen, J.Y.; Xie, Z.H.; Li, W.N.; Lin, S.B.; Zhang, L.L.; Liu, C.X. Construction and investigation of a planar waveguide in photo-thermal-refractive glass by proton implantation. *Optik* **2020**, *207*, 164461. [CrossRef]
8. Revathi, V.; Rajendran, V. Investigation about nonlinear optics and antibacterial activity of pyrrolidine-2-carboxylic acid cadmium chloride hydrate single crystal. *Optik* **2018**, *154*, 234–241. [CrossRef]
9. Liu, C.X.; Shen, X.L.; Guo, H.T.; Li, W.N.; Wei, W. Proton-implanted optical waveguides fabricated in Er^{3+}-doped phosphate glasses. *Optik* **2017**, *131*, 132–137. [CrossRef]
10. Koutsoumpos, S.; Giannios, P.; Moutzouris, K. Extended derivative method of critical-angle refractometry for attenuating media: Error analysis. *Meas. Sci. Technol.* **2021**, *32*, 105007. [CrossRef]
11. Zeng, H.; Wang, J.; Ye, Q.; Deng, Z.; Mei, J.; Zhou, W.; Zhang, C.; Tian, J. Study on the refractive index matching effect of ultrasound on optical clearing of bio-tissues based on the derivative total reflection method. *Biomed. Opt. Express* **2014**, *5*, 3482. [CrossRef]
12. Sun, T.Q.; Ye, Q.; Wang, X.W.; Wang, J.; Deng, Z.C.; Mei, J.C.; Zhou, W.Y.; Zhang, C.P.; Tian, J.G. Scanning focused refractive-index microscopy. *Sci. Rep.* **2014**, *4*, 5647. [CrossRef]
13. Meeten, G.H.; North, A.N.; Willmouth, F.M. Errors in critical-angle measurement of refractive index of optically absorbing materials. *J. Phys. E Sci. Instrum.* **1984**, *17*, 642–643. [CrossRef]
14. Goyal, K.G.; Dong, M.L.; Kane, D.G.; Makkar, S.S.; Worth, B.W.; Bali, L.M.; Bali, S. Note: Refractive index sensing of turbid media by differentiation of the reflectance profile: Does error-correction work? *Rev. Sci. Instrum.* **2012**, *83*, 086107. [CrossRef]
15. Morales-Luna, G.; García-Valenzuela, A. Viability and fundamental limits of critical-angle refractometry of turbid colloids. *Meas. Sci. Technol.* **2017**, *28*, 125203. [CrossRef]
16. Giannios, P.; Toutouzas, K.G.; Matiatou, M.; Stasinos, K.; Konstadoulakis, M.M.; Zografos, G.C.; Moutzouris, K. Visible to near-infrared refractive properties of freshly-excised human-liver tissues: Marking hepatic malignancies. *Sci. Rep.* **2016**, *6*, 27910. [CrossRef]
17. Giannios, P.; Koutsoumpos, S.; Toutouzas, K.G.; Matiatou, M.; Zografos, G.C.; Moutzouris, K. Complex refractive index of normal and malignant human colorectal tissue in the visible and near-infrared. *J. Biophotonics* **2016**, *10*, 303–310. [CrossRef] [PubMed]
18. Räty, J.; Pääkkönen, P.; Peiponen, K.E. Assessment of wavelength dependent complex refractive index of strongly light absorbing liquids. *Opt. Express* **2012**, *20*, 2835. [CrossRef] [PubMed]
19. Koutsoumpos, S.; Giannios, P.; Stavrakas, I.; Moutzouris, K. The derivative method of critical-angle refractometry for attenuating media. *J. Opt.* **2020**, *22*, 075601. [CrossRef]
20. Meeten, G.H. Refractive index errors in the critical-angle and the Brewster-angle methods applied to absorbing and heterogeneous materials. *Meas. Sci. Technol.* **1997**, *8*, 728–733. [CrossRef]
21. Kedenburg, S.; Vieweg, M.; Gissibl, T.; Giessen, H. Linear refractive index and absorption measurements of nonlinear optical liquids in the visible and near-infrared spectral region. *Opt. Mater. Express* **2012**, *2*, 1588. [CrossRef]
22. Ninni, P.D.; Martelli, F.; Zaccanti, G. Intralipid: Towards a diffusive reference standard for optical tissue phantoms. *Phys. Med. Biol.* **2010**, *56*, N21–N28. [CrossRef] [PubMed]
23. Zhao, Y.; Qiu, L.; Sun, Y.; Huang, C.; Li, T. Optimal hemoglobin extinction coefficient data set for near-infrared spectroscopy. *Biomed. Opt. Express* **2017**, *8*, 5151. [CrossRef] [PubMed]
24. Zhao, D.; Zhang, G.; Zhang, X.; Li, D. Optical properties of paraffin at temperature range from 40 to 80 °C. *Optik* **2018**, *157*, 184–189. [CrossRef]
25. Forouhi, A.R.; Bloomer, I. Optical properties of crystalline semiconductors and dielectrics. *Phys. Rev. B* **1988**, *38*, 1865–1874. [CrossRef]
26. Li, X.; Zhao, J.M.; Wang, C.C.; Liu, L.H. Improved transmission method for measuring the optical extinction coefficient of micro/nano particle suspensions. *Appl. Opt.* **2016**, *55*, 8171. [CrossRef]
27. Ninni, P.D.; Martelli, F.; Zaccanti, G. Effect of dependent scattering on the optical properties of Intralipid tissue phantoms. *Biomed. Opt. Express* **2011**, *2*, 2265. [CrossRef]

28. Feder, I.; Duadi, H.; Fixler, D. Single wavelength measurements of absorption coefficients based on iso-pathlength point. *Biomed. Opt. Express* **2020**, *11*, 5760. [CrossRef]
29. Marchesini, R.; Bertoni, A.; Andreola, S.; Melloni, E.; Sichirollo, A.E. Extinction and absorption coefficients and scattering phase functions of human tissues in vitro. *Appl. Opt.* **1989**, *28*, 2318. [CrossRef] [PubMed]
30. Ogusu, K.; Suzuki, K.; Nishio, H. Simple and accurate measurement of the absorption coefficient of an absorbing plate by use of the Brewster angle. *Opt. Lett.* **2006**, *31*, 909. [CrossRef]
31. Wu, S.; Lian, J.; Song, P.; Gao, S.; Wang, X.; Ma, Z.; Wang, Y.; Guan, W. Optical properties of $Sr_3NbGa_3Si_2O_{14}$ crystal. *Opt. Int. J. Light Electron Opt.* **2013**, *124*, 686–688. [CrossRef]
32. Zhou, W.; Zhou, Y.; Albert, J. A true fiber optic refractometer. *Laser Photonics Rev.* **2017**, *11*, 1600157. [CrossRef]